Fracture Surface Morphology in Thermosets Modified with Hollow Microspheres

Ho Sung Kim

Discipline of Mechanical Engineering, School of Engineering, The University of Newcastle, Callaghan, New South Wales 2308, Australia

Received 8 October 2006; accepted 25 February 2007
DOI 10.1002/app.26596
Published online 24 May 2007 in Wiley InterScience (www.interscience.wiley.com).

ABSTRACT: Fracture surface morphology in relation with toughening of thermosets modified with hollow microspheres was studied. Two different toughening methods were employed—one was with (MEH) and the other without (ME) compressive residual stresses around microspheres, respectively. The compressive residual stresses were to increase effective stress intensity factor. Various conditions arising from toughening method, properties of constituent materials, bonding between matrix and microspheres, relativity between bonding and microsphere strengths, and plane stress/strain were derived for part of generalization of fracture surface morphology. Mohr circle representations were employed for relative stress components analysis. New deformation mechanisms contributing to toughening were proposed. A major difference in toughening mechanism between ME and MEH methods was found to be in the location of plastic deformation under plane strain. The plastic deformation of ME was dominantly in matrix and appeared in the form of matrix cavitation. In the case of MEH, it was dominantly in microspheres. It was suggested that compressive residual stress promotes plastic deformation of microspheres caused by ''extrusion'' effect. The microsphere deformation in MEH was found also under plane stress although it was not as much as under plane strain. Matrix cavitation in ME under plane stress, however, was not found. J Appl Polym Sci 105: 3287–3294, 2007

Key words: thermosets; composites; fracture; toughness; stress

INTRODUCTION

Thermosets are an important family of engineering plastics. They are, however, brittle compared to thermoplastics because of their crosslinked molecular structures. Much effort has been made to improve such weakness particularly for epoxies. Liquid rubber has been used as a modifier owing to its remarkable toughening effect not only for themosets but also for thermoplastics.[1–3] Toughening mechanisms due to the liquid rubber have been studied by numerous researchers since Sultan and McGarry[4] found its toughening effect. The toughening mechanisms include cavitation and shear banding,[5] crack pinning,[6] bridging,[7] crack blunting[8] etc. Pearson and Yee[9] suggested that major toughening mechanisms contributing to the improvement of toughness are cavitation and shear deformation between rubber particles. Another development in toughening is some attempts using a similar method to the one used for ceramics in which toughness increase was achieved by volume dilation in the vicinity of the crack tip resulted from tetragonal to monoclinic phase transformation.[10,11] Kim and Robertson[12–14] have investigated toughening with semicrystalline thermoplastic polymers as modifiers and as a result substantial toughening has been achieved. They thought phase transformation was the major toughening mechanism but it was inconclusive.[12] Some variation of toughening mechanisms has been achieved using other modifiers such as glass beads,[15–17] hollow micro-spheres,[18–21] and core-shell rubber[22] and voids.[23]

Recently, Kim and Kim[24–28] have developed a new toughening method to increase the effective critical stress intensity factor by purposely producing compressive prestresses around microspheres. The compressive prestresses in the matrix were produced by expansion of microspheres containing gas. The toughening method has already been demonstrated to be efficient. However, its detailed study on deformation mechanism leading to fracture surface morphology, which might provide a salient insight into the toughening, has not been conducted. The deformation, in general, is controlled by hydrostatic and deviatoric stress components. The hydrostatic stress component does not cause plastic deformation but contributes to elastic volume changes whereas the deviatoric stress component involves in causing plastic deformation. The two stress components can be related to each other and represented by the Mohr circle.[29] In the present work, deformation mecha-

Correspondence to: H. S. Kim (ho-sung.kim@newcastle.edu.au).

Journal of Applied Polymer Science, Vol. 105, 3287–3294 (2007)

nisms of both prestressing and nonpre-stressing methods will be further studied within a framework of various conditions with Mohr circle analysis.

Conditions affecting fracture surface morphology

In general, fracture surface morphology of particulate composites is dependant upon various properties for interface between matrix and filler particles, filler particles, and matrix. Also it depends on toughening method involving precompression or nonprecompression, and on stress state.

Possible bond conditions of the interface between matrix and filler particles due to cavitation in the vicinity of the crack tip at which the hydrostatic component is at its maximum under plane strain are

fully bonded, (c1)

partially bonded, and (c2)

fully debonded. (c3)

When microspheres are fully debonded, their role in toughening is equivalent to that of voids[23] and interaction with matrix no longer occurs.

Possible property conditions for filler particles and matrix are

$$E_m > E_p, \tag{c4}$$

$$E_m = E_p \tag{c5}$$

and

$$E_m < E_p, \tag{c6}$$

where E_m is the elastic modulus of matrix and E_p is the elastic modulus of filler particle. Poisson's ratios would affect the hydrostatic component to some extent and should be included if rigorous analysis would be applied.

Possible relativity conditions at the crack tip between matrix and particle at fracture are

$$F_b > F_m > F_p, \tag{c7}$$

$$F_b > F_p > F_m, \tag{c8}$$

$$F_b < F_m < F_p \tag{c9}$$

and

$$F_b < F_p < F_n \tag{c10}$$

where F_b is the maximum bonding force between matrix and filler particle resisting the applied load, F_m is the maximum force matrix can carry until it fails, and F_p is the maximum force a particle can carry until it fails. When the condition c7 occurs, filler particle fails whereas when condition c8 occurs, matrix fails. When the condition c9 or c10 occurs, only debonding takes place. The interface bonding is usually ill defined due to the difficulty of the small scale characterization but postmortem examination on fracture surface provides useful information. Also, interface bonding can be controlled to some extent by coating[30] or chemically.[31]

In this way, 144 different combinations (=2 [toughening methods] × 3 [bond conditions due to cavitation] × 3[elastic moduli] × 4 [bonding at the crack tip] × 2 [plane stress/strain]) arising from different conditions are possible, leading to various morphologies.

Some deformation contributing to toughness can intuitively be described. Matrix deformation, for example, is expected to be larger for either low interface bonding strength or low elastic modulus of filler particle because the constraint in the vicinity of the crack tip caused by either of those properties on matrix is weak. Deformation of filler particles in relation with various conditions and relative quantities, however, is no longer intuitive. Some aspects of the relativity of various conditions will be further discussed with experimental results.

EXPERIMENTAL

Experimental details from Ref. 26 are included here to be self-sufficient within the scope of the paper.

Materials used

An epoxy system was adopted as a model material for this study. The system consisted of West System Epoxy 105 (a blend of Bisphenol A and Bisphenol F) and West System Slow Hardener 206 (a blend of aliphatic amines and aliphatic amine adducts based on diethylene triamine and triethylenetetramine) as curing agent. An average density of five measurements was found to be 1.1 g/cc for the epoxy system.

Modifier particles used were preformed hollow microspheres (EXPANCEL, 551 DU40, Akzo Nobel) which consist of copolymer shell and gas. The microspheres were analyzed for chemical structure using a Perkin–Elmer Fourier Transform Infra Red Spectrometer (Paragon 1000) and found to be $(C_5H_8O_2—C_3H_3N—C_2H_2Cl_2)x$. An average density of microspheres from three measurements at room temperature was found, using an air comparison pycnometer (Beckman 930), to be 1.2. The hollow microsphere sizes were measured using a laser particle analyzer (Malvern 2600C) and their size distribution is given in Figure 1.

The microspheres expand when heated. As part of characterization for volume expansion of 551 DU40, 10 mL microspheres were put in a 100 mL mea-

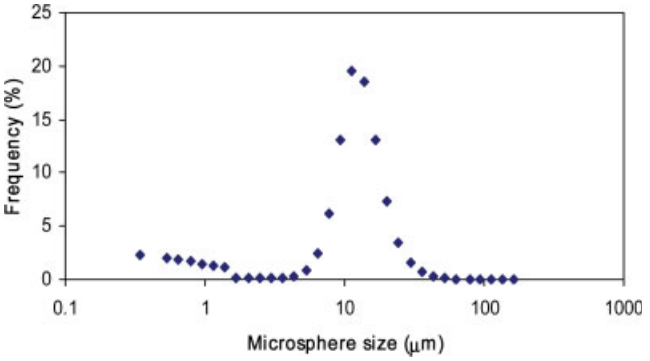

Figure 1 Hollow microsphere size distribution. [Color figure can be viewed in the online issue, which is available at www.interscience.wiley.com.]

suring cylinder and tapped for 5 min and then placed in an oven preheated to 70°C. Further heating followed every 5–6 min for an increment of 10°C until it reached 200°C. The volume expansion as a function of temperature is shown in Figure 2. It is seen that the volume reaches its maximum and then decreases because some hollow microspheres explode when the temperature is high.

Manufacturing process for modification with microspheres

Modification of epoxy in two different ways was conducted i.e., one is without heat treatment (ME) and the other with heat treatment (MEH). The heat treatment was to produce compressive stresses around microspheres. The details are as follows. Microspheres were first added to epoxy and stirred for about 10 min. The mixture was heated to about 80°C for 30 min to reduce the viscosity for easy stirring and then allowed to cool in a water bath for about half an hour. The hardener 17 phr (by weight) was then added and stirred for 5 min. The resulting mixture was poured into an aluminum mold with a cavity of 6 × 150 × 150 mm^3 and left for curing at room temperature at least for one day for ME specimens. (Temperature rise in the mold due to exothermic reaction was monitored using a thermocouple and found to be about 8°C which would not affect the expansion of hollow microspheres.) Further, heat treatment was conducted on demoulded specimens for MEH in an oven at 135°C for 2 h and then allowed to cool down to room temperature.

Mechanical testing

All the specimens for mechanical testing were machined into dimensions of 12 × 60 × 6 mm^3 for edgewise placement. Three point bending tests on a universal testing machine (Shimadzu 5000) were conducted for elastic modulus, strength, and fracture toughness. A crosshead speed of 10 mm/min was adopted for tests of flexural properties and 0.5 mm/min for the fracture toughness measurements at a room temperature of 21°C.

The critical stress intensity factor (K_{IC}) expression[32] used was

$$K_{IC} = \frac{3PS\sqrt{\pi a}}{2BW^2} Y \tag{1}$$

where a is the crack length and Y is a geometry factor given by

$$Y = \frac{1}{\sqrt{\pi}} \frac{1.99 - \frac{a}{W}\left(1 - \frac{a}{W}\right)\left(2.15 - 3.93\frac{a}{W} + 2.7\left(\frac{a}{W}\right)^2\right)}{\left(1 + 2\frac{a}{W}\right)\left(1 - \frac{a}{W}\right)^{3/2}}. \tag{2}$$

Specific fracture energy values for mode I were approximated using

$$G_{IC} = \frac{K_{IC}^2}{E}. \tag{3}$$

It is noted that load-displacement curves obtained were at least approximately linear as already shown elsewhere[27] and this approximation may be conservative for any nonlinear behavior.

A precrack up to 6 mm long was produced by a tapping a razor blade into the tip of 2 mm long saw-cut notch.

Microscopy

Scanning electron microscopic (SEM) work using a JEOL JSM-840 (tungsten filament, 10 kV) was conducted. Fractured samples were cleaned with water in an ultrasonic cleaner (Bran Sonic 52) and dried in an oven at 30°C for 30 min. Samples were gold coated using a SPI-MODULE™ Sputter Coater at 10 mA for 4 min. Images were taken for approximate locations A and B (Fig. 3)—location A is close to sur-

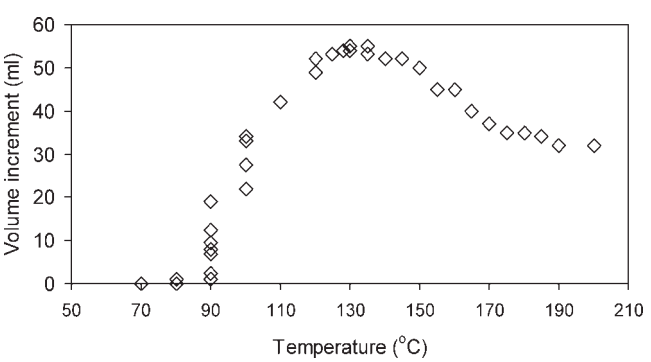

Figure 2 Volume expansion measurement of 551 DU40 as a function of temperature.[26]

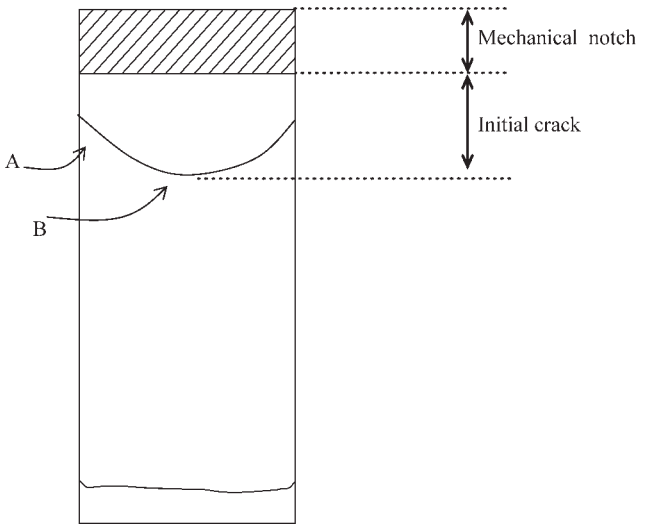

Figure 3 Approximate locations of SEM fracture surface images taken for plane stress (A) and plane strain (B).

face and hence regarded as plane stress dominant, and location B is far from the surface and hence regarded as plain strain dominant.

RESULTS AND DISCUSSION

Fracture toughness in both K_{IC} (critical stress intensity factor) and G_{IC} (critical specific fracture energy) is given in Figure 4. Both ME and MEH increase in toughness as micro-sphere content increases up to a content of 20 phr and thereafter tend to be relatively flat or slightly decrease. MEH appears a little higher than ME in K_{IC} reflecting the increase in effective stress intensity due to precompressive stresses around microspheres in the case of MEH. Also, MEH further appears much higher than ME in G_{IC} indicating that much more deformation occurred in MEH than in ME at fracture according to Eq. (3).

SEM images of fracture surfaces of ME are given in Figure 5 for both plane stress and strain. A major difference between plane stress [Fig. 5(a)] and plane strain [Fig. 5(b)] appears to be in interface bonding between microspheres and matrix. Some gaps between microspheres and matrix are seen on fracture surface formed under plane strain. The gaps were previously discussed in relation with two pos-

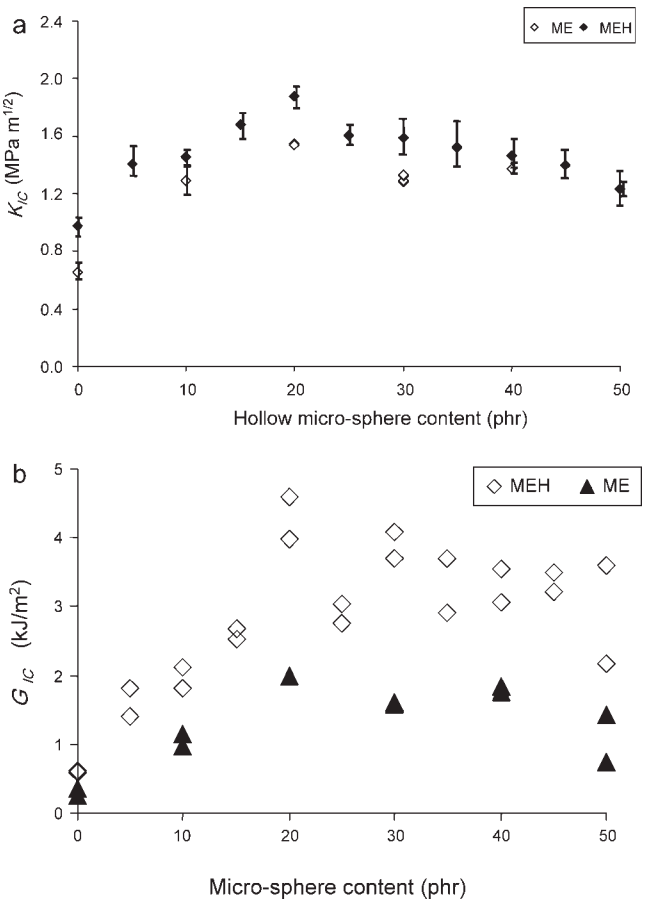

Figure 4 Fracture toughness as a function of hollow microspheres for ME and MEH series: (a) critical stress intensity factor (K_{IC})[27] and (b) specific fracture energy (G_{IC}).[26]

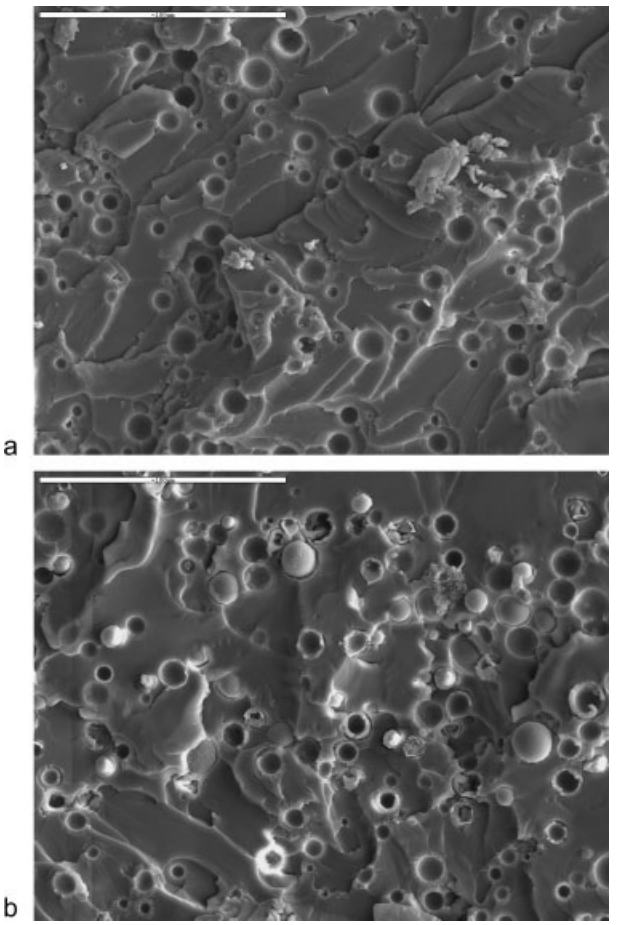

Figure 5 SEM images of fracture surfaces in the vicinity of initial crack tip of ME, 15 phr: (a) plane stress, and (b) plane strain. Crack propagation direction is from top to bottom. Each scale bar represents 100 μm.

sibilities—one is due to cavitation and the other epoxy shrinkage[26] and it was deduced to be due to the cavitation of matrix. In contrast, no gaps under plane stress are seen and the fracture surface suggests that the crack passed through microspheres without pull-outs of microspheres. (Cavitation would not likely occur under plane stress because stress state is more biaxial than triaxial and hence less hydrostatic stress component.) This finding supports the previous deduction[26] that the gaps are due to cavitation of matrix. Further, the features of microspheres found on fracture surface under plane strain include the following three types:

a. partially debonded from matrix and broken with torn marks on fracture surfaces (conditions c2 and c7);
b. fully debonded and pulled out from matrix (conditions c3 and c9 or c10)); and
c. fully bonded but broken with relatively flat fracture surfaces (conditions c1 and c7).

The three types are further schematically illustrated in Figure 6 for clarity. The first and last types of microsphere deformation will be discussed using the Mohr circle as follows. When the crack tip approaches a microsphere as a result of crack propagation, two different bonding conditions (c1 and c2) as illustrated in Figure 7(a,b) may be considered in the vicinity of the crack and relevant Mohr circles can be constructed. The normal stress components in x, y, and z directions (σ_x, σ_y, and σ_z) in the Mohr circle [Fig. 7(a)] represent the principal stresses on x axis. It is known that $\sigma_y > \sigma_z > \sigma_x$ in the vicinity of the crack under plane strain when no precompressive stress exists.[33] The location of σ_z [$= v(\sigma_x + \sigma_y)$] on the normal stress (σ) axis for the Mohr circle depends on Poission's ratio, v. First, when the microsphere is ''partially debonded'' possibly due to cavitation [Fig. 7(b)] with conditions c2 and c7, the normal stress components (σ_x, σ_y, and σ_z) in Figure 7(a) become (σ'_x, σ'_y, and σ'_z) respectively, in Figure 7(b) as a result of relief of the three stress components (i.e., $\sigma'_x < \sigma_x$, $\sigma'_y < \sigma_y$, $\sigma'_z < \sigma_z$), and also the hydrostatic component acting on the microsphere is shown to be

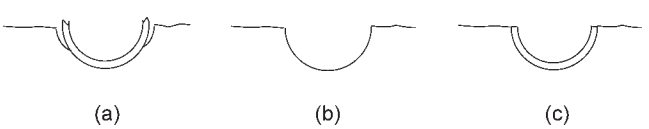

Figure 6 Schematic representation of microsphere cross sections in matrix under plane strain for ''Figure 5(b)'': (a) partially debonded and broken with torn marks; (b) fully debonded and pulled out from matrix; and (c) fully bonded but broken without torn marks.

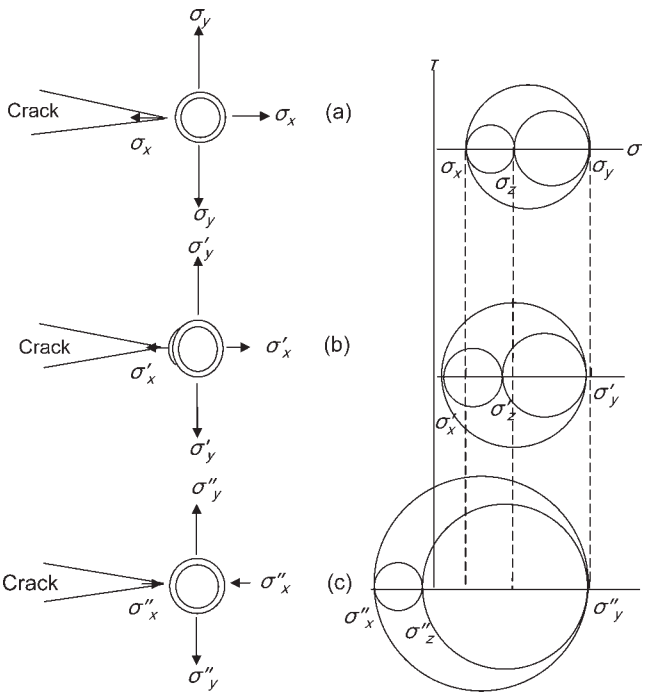

Figure 7 Microsphere cross sections with relative stress components in the vicinity of the crack tip and corresponding Mohr circles under plane strain: (a) fully bonded for ME, (b) partially debonded for ME, and (c) fully bonded for MEH. τ is the shear stress.

relatively small due to the relief of other stress components in mainly x- and z-directions, i.e.

$$(\sigma'_x + \sigma'_y + \sigma'_z)/3 < (\sigma_x + \sigma_y + \sigma_z)/3. \quad (4)$$

Consequently, some plastic deformation and torn marks are expected in the case of Figure 7(b), given the higher deviatoric stress component the more ductile. (The condition c4 in this case is assumed because microsphere is highly deformable[26]). Second, when a microsphere is ''fully bonded'' [Fig. 7(a)], constraint on the microsphere is not much relieved and hence the hydrostatic component is highly retained, resulting in relatively brittle failure of microspheres as evidenced by flat fracture surfaces of microspheres (Fig. 5). The relative difference between two bonding conditions [Fig. 7(a,b)] may be given by

$$|\sigma_x - \sigma'_x| (\text{or } |\sigma_z - \sigma'_z|) > |\sigma_y - \sigma'_y| \quad (5)$$

depending on the location and size of debonded area.

Figure 8 shows SEM images of fracture surfaces in the vicinity of initial crack tip of MEH. When a specimen is heated, microspheres naturally expand against matrix and both matrix and microspheres would permanently deform if deformation is suffi-

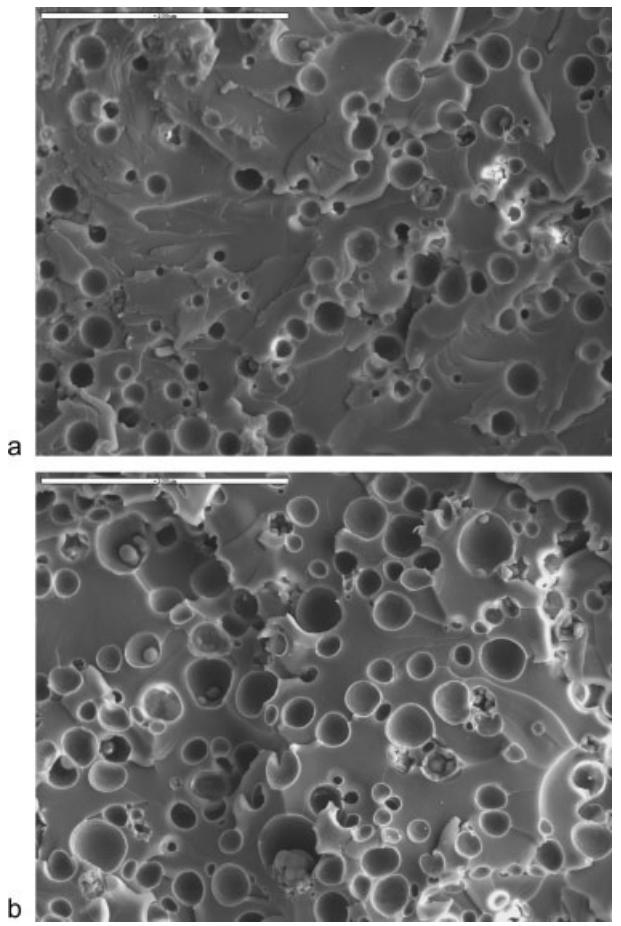

Figure 8 SEM images of fracture surfaces in the vicinity of initial crack tip of MEH, 15 phr: (a) plane stress, and (b) plane strain. The crack propagation direction is from top to bottom. Each scale bar represents 100 μm.

ciently high. Consequently, compressive residual stresses around microspheres are created when cooled down. As typical fracture surface features of MEH previously also shown in Ref. 26 major features of this method of toughening include thin edges of broken microspheres, indicating that microspheres experienced large deformation without debonding as also illustrated schematically in Figure 9. Such large deformation in MEH occurred in both plane stress [Fig. 8(a)] and plane strain [Fig. 8(b)]. The only difference between plane stress and plane strain is that the large deformation (thin edges) is less prominent under plane stress—some of microspheres under plane stress are seen to be neither such largely deformed nor noticeably deformed. Another feature to notice in deformation in MEH is that microspheres are not as much spherical as those in ME but rather distorted. Given that polished thin section[26] revealed that microspheres are spherical, the distortion seems to have occurred after cracking. One of possibilities of such large deformation may be due to property change of microspheres. However, this possibility can be eliminated because some microspheres under plane stress [Fig. 8(a)] do not seem to be much deformed, indicating that the heated treatment did not cause such property change. Thus, the large deformation appears to be caused by a stress condition when fracture occurs rather than property change of microspheres.

Now, the conditions, c1, c4, and c7 can be applicable to MEH and deformation mechanism of microspheres can be related to relative stress components of matrix under plane strain by constructing Mohr circles shown in Figure 10. When a microsphere is sufficiently far away from the crack [Fig. 10(b)], compressive hydrostatic component acting on the microsphere is at its maximum but deviatoric stress component is at its minimum (zero) since

$$\sigma_y'' = \sigma_z'' = \sigma_x'' \tag{6}$$

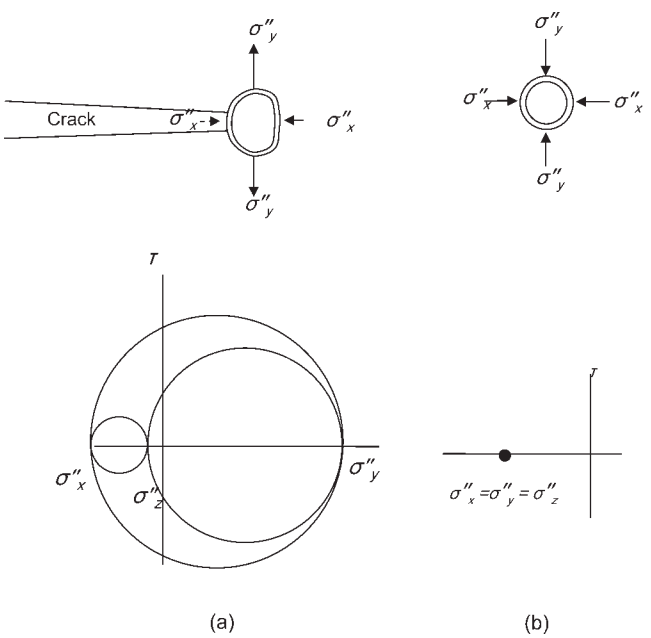

Figure 10 Microsphere cross section with stress components and Mohr circles under plane strain for MEH: (a) microsphere at the crack tip, and (b) microsphere far away from the crack tip with a corresponding point representing a Mohr circle representation for $\sigma_x'' = \sigma_y'' = \sigma_z''$. The stress component in the z-direction (σ_z'') is omitted in illustration around microspheres.

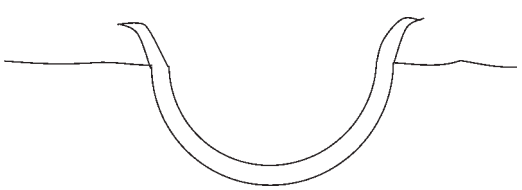

Figure 9 Schematic representation of a microsphere cross section with matrix for a large deformation after fracture.

at a location under plane strain. However, as the crack propagates and it reaches a microsphere as shown in Figure 10(a), some of the hydrostatic component acting on microspheres progressively decreases with increasing deviatoric stress component as y-direction stress component (σ''_y) more rapidly increases than other stress components (σ''_y and σ''_z) and eventually compressive σ''_y becomes tensile σ''_y. The stress components in x and z directions (σ''_x and σ''_z), however, retain relatively high residual stress components because σ''_x and σ''_z caused by loading are small compared to σ''_y. Thus, the residual stresses contribute to the large radius of Mohr circle by increasing deviatoric stress component. The Mohr circle based on this discussion for a microsphere fully bonded prior to large deformation is also given in Figure 7(c) in comparison with ones discussed previously. The y-direction stress components are found to be at least approximately

$$\sigma''_y = \sigma_y \tag{7}$$

according to the maximum principal stress fracture criterion[34] and that the difference, $|\sigma''_x - \sigma_x|$ or $|\sigma''_z - \sigma_z|$, represents initially created compressive residual stress with

$$|\sigma''_x - \sigma_x| = |\sigma''_z - \sigma_z|. \tag{8}$$

It can be found in the Mohr circle that elongation of microsphere in y-direction can be increased by decreasing the quotient,

$$|\sigma''_z - \sigma''_x|/|\sigma''_y - \sigma''_x| \tag{9}$$

and also by increasing compressive residual stress. It can thus be suggested that the large plastic deformation (thin edges) of microspheres (Fig. 8) is the result from ''extrusion'' (elongation in a particular direction) effect caused by the compressive residual stress. Also the extrusion effect leads to small pulling force on the microsphere at fracture, resulting in low chance of debonding as taken place in MEH. In the case of plane stress ($\sigma''_z = 0$), the extrusion effect is expected to be as not much strong as that under plane strain in the presence of x-direction residual stress according to the quotient[9] as evidenced in Figure 8.

CONCLUSIONS

Various toughening conditions resulting from different toughening methods, properties of constituent materials, bonding between matrix and microspheres, relativity between bonding and microsphere strengths, and plane stress/strain have been suggested as a part of generalized framework for understanding deformation mechanisms and morphology of fracture surfaces.

New deformation mechanisms contributing to toughness in relation with the aforementioned toughening conditions, relative stress components, and fracture morphology have been proposed and analyzed using Mohr circles.

A major difference in toughening between ME and MEH methods was found to be in the location of plastic deformation under plane strain. The plastic deformation of ME was dominantly in matrix and appeared in the form of matrix cavitation. In the case of MEH, it was dominantly in microspheres. It was suggested that compressive residual stress promotes plastic deformation of microspheres caused by ''extrusion'' effect. The microsphere deformation in MEH was found also under plane stress although it was not as much as that under plane strain. Matrix cavitation in ME under plane stress, however, was not found.

The author thanks Ms N. Muthubandara and Mr D. Phelan for the assistance with SEM photographs. Part of this paper was invited and presented in a plenary session at an International Composites Conference, ACUN-5, Developments in Composites: Advanced, Infrastructural, Natural, and Nano-Composites, Sydney, Australia, 11-14 July 2006.

References

1. Wu, S. Polymer 1985, 26, 1855.
2. Wu, S. J Appl Polym Sci 1988, 35, 549.
3. Kim, N. H.; Kim, H. S. J Appl Polym Sci 2006, 101, 4256.
4. Sultan, J. N.; McGarry, F. J. J Polym Eng Sci 1973, 13, 29.
5. Yee, A. F.; Pearson, R. A. J Mater Sci 1986, 24, 2475.
6. Lange, F. F.; Philos Mag 1970, 22, 983.
7. Kunz-Douglass, S.; Beaumont, P. W. R.; Ashby, M. F. J Mater Sci 1980, 15, 1109.
8. Kinloch, A. J.; Williams, J. G. J Mater Sci 1980, 15, 987.
9. Pearson, R. A.; Yee, A. F. J Mater Sci 1986, 21, 2475.
10. Garvie, R. C.; Hannink, R. H.; Pascoe, R. T.; Nature 1975, 258, 703.
11. Hannink, R. H.; Kelly, P. M.; Muddle, B. C. J Am Ceramic Soc 2000, 83, 461.
12. Pearson, R. A. In Toughened Plastics I—Science and Engineering; Riew, C. K.; Kinloch, A. J., Eds.; Advance in Chemistry Series 233; American Chemical Society: Washington, DC, 1993, p 405.
13. Kim, J. K.; Robertson, R. E. J Mater Sci 1992, 27, 161.
14. Kim, J. K.; Robertson, R. E. J Mater Sci 1992, 27, 3000.
15. Lee, J.; Yee, A. F. Polymer 2000, 41, 8363.
16. Lee, J.; Yee, A. F. Polymer 2001, 42, 577.
17. Lee, J.; Yee, A. F. Polymer 2001, 42, 589.
18. Bagheri, R.; Pearson, R. A. Polymer 1995, 36, 4883.
19. Bagheri, R.; Pearson, R. A. Polymer 1996, 37, 4529.
20. Bagheri, R.; Pearson, R. A. Polymer 2000, 41, 269.
21. Kim, H. S.; Khamis, M. A. Compos Part A: Appl Sci Eng 2001, 32, 1311.

22. Xiao, K.; Ye, L. Polym Eng Sci 2000, 40, 70.
23. Kim, N. H.; Kim, H. S. J Appl Polym Sci 2005, 98, 1290.
24. Kim, N. H.; Kim, H. S. ANTEC 2003, May 4–7, Nashville, Tennessee, USA, Vol. 2, p 2069.
25. Kim, H. S.; Kim, N. H. Int. Pat. PCT/AU03/00250 (2004).
26. Kim, N. H.; Kim, H. S. J Appl Polym Sci 2005, 98, 1663.
27. Kim, H. S.; Kim, N. H. J Appl Polym Sci 2006, 100, 4045.
28. Kim, N. H.; Kim, H. S. J Appl Polym Sci 2006, 100, 4470.
29. Dieter, G. E. Mechanical Metallurgy, 2nd ed.; McGraw-Hill: New York, 1976.
30. Amdouni, N.; Sautereau, H.; Gerard, J. F.; Fernagut, F.; Coulon, G.; Lefebvre, J. M. J Mater Sci 1990, 25, 1435.
31. Huang, Y.; Kinloch, A. J.; Bertsch, R. J.; Siebert, A. R. In Toughened Plastics I; Riew, C. K.; Kinloch, A. J., Eds. Advance in Chemistry Series 233; American Chemical Society: Washington, DC, 1993; p 189.
32. Tada, H.; Paris, P. C.; Irwin, G. R. The Stress Analysis of Cracks Handbook, 2nd ed.; Paris Productions: St Louis, 1985.
33. Broek, D. Elementary Engineering Fracture Mechanics, Sijthoff & Noordhoff: The Netherlands, 1978.
34. Erdogan, F.; Sih, G. C. J. Basic Eng 1963, December, 519.